SCIENCE CHINA Materials ARTICLES

mater.scichina.com link.springer.com

Published online 27 October 2017 | https://doi.org/10.1007/s40843-017-9098-2

Sci China Mater 2018, 61(4): 545–556

SPECIAL ISSUE: Advances in Metallic Biomaterials

Preparation and bioactive surface modification of the microwave sintered porous Ti-15Mo alloys for biomedical application

Jilin Xu[1*], Jinlong Zhang[1], Luzi Bao[1], Tao Lai[1], Junming Luo[1] and Yufeng Zheng[2*]

ABSTRACT **Biomedical porous Ti-15Mo alloys were prepared by microwave sintering using ammonium hydrogen carbonate (NH_4HCO_3) as the space holder agent to adjust the porosity and mechanical properties. The porous Ti-15Mo alloys are dominated by β-Ti phase with a little α-Ti phase, and the proportion of α and β phase has no significant difference as the NH_4HCO_3 content increases. The porosities and the average pore sizes of the porous Ti-15Mo alloys increase with increase of the contents of NH_4HCO_3, while all of the compressive strength, elastic modulus and bending strength decrease. However, the compressive strength, bending strength and the elastic modulus are higher or close to those of natural bone. The surface of the porous Ti-15Mo alloy was further modified by hydrothermal treatment, after which $Na_2Ti_6O_{13}$ layers with needle and flake-like clusters were formed on the outer and inner surface of the porous Ti-15Mo alloy. The hydrothermally treated porous Ti-15Mo alloy is completely covered by the Ca-deficient apatite layers after immersed in SBF solution for 14 d, indicating that it possesses high apatite-forming ability and bioactivity. These results demonstrate that the hydrothermally treated microwave sintered porous Ti-15Mo alloys could be a promising candidate as the bone implant.**

Keywords: porous Ti-15Mo alloy, microwave sintering, hydrothermal treatment, apatite-forming ability, mechanical property

INTRODUCTION

With the increase of trauma, deformity, degeneration and an aging population, the demand of human hard tissue (such as bones, knee joints and dental roots) replacement materials has rapidly grown, which greatly stimulates the development of biocompatible implant materials [1]. Among the traditional metallic biomaterials, titanium and its alloys are the most attractive due to their high specific strength, excellent biocompatibility and superior corrosion resistance [2–4]. However, these advantages are not enough to avoid failure risks of bone implants, because there are three main issues to be solved, stress shielding effect, biological safety and bioactivity. The mismatch of the elastic modulus between the Ti alloys (90–110 GPa) and natural bone (<30 GPa) can cause serve "stress shielding" effect, which results in the bone resorption, implant loosening and eventual failure [4–6]. The cytotoxic Al or V ions released from the Ti alloys implant into the human body fluid might cause long-term potential biological problems [7–9]. The bioinert Ti alloys not only cannot form enough osseointegration, but also are generally encapsulated by fibrous tissue and separated from the surrounding bone, which results in a deficient biomechanical fixation and clinical failure of the implant [4,10,11].

In order to relieve the problems of stress shielding effect and the cytotoxic elements, near β type titanium alloys composed of non-toxic elements like Ti-Mo, Ti-Nb-Zr, Ti-Nb-Zr-Ta and Ti-Ta alloys, have emerged as one of the most promising materials for load-bearing biomedical materials due to their high strength, low elastic modulus, good corrosion resistance and excellent biocompatibility [8,12–15]. Among these, Ti-15Mo alloy has been listed as a potential biomaterial by the American Society for Testing and Materials (ASTM) [16] due to its excellent integrated mechanical properties and biological properties [8,17–19]. Moreover, introducing pores into

[1] School of Materials Science and Engineering, Nanchang Hangkong University, Nanchang 330063, China
[2] State Key Laboratory for Turbulence and Complex System and Department of Materials Science and Engineering, College of Engineering, Peking University, Beijing 100871, China
[*] Corresponding authors (emails: jlxu@nchu.edu.cn (Xu J); yfzheng@pku.edu.cn (Zheng Y))

the bulk Ti alloys and forming the porous materials is a more efficient method to lower their elastic modulus [1,5,20–22]. Especially, porous structure could not only provide the adjustable elastic modulus and improve the biomechanical compatibility of the implants, but also allow the ingrowth of new bone tissue and vascularization and a firm fixation of the implants could be obtained [1,5,20–22].

Recently, there are some reports about the porous Ti-Mo alloys prepared by different methods, such as vacuum sintering [9,10], gelcasting [23], selective laser sintering [24,25] and atmosphere protection conventional sintering [21,26]. Microwave sintering is a new powder metallurgy sintering method to prepare the porous metallic materials, such as porous NiTi alloys [27,28], porous Ti6Al4V/TiC/HA composites [29] and porous Ti/CaP composites [30]. It depends on the powders of the compacts coupling with microwaves, absorbing the electromagnetic energy volumetrically, transforming into heat up to sintering temperature and realizing the densification and alloying eventually [31–33]. Compared with conventional sintering, the microwave sintering possesses many intrinsic advantages, such as reduced energy consumption, rapid heating rates, reduced sintering times, enhanced element diffusion processes and improved physical and mechanical properties of the sintered materials [31–33]. Unfortunately, to the best of our knowledge, studies on the microwave sintering to prepare the porous Ti-Mo alloys have not been reported in literature.

Surface modification is the most efficient method to improve the bioactivity and osseointegration of the implant materials. So far, several surface modification methods have been employed to activate the Ti-Mo alloys, such as thermal oxidation [18], plasma electrolytic oxidation [34,35], anodic oxidation [36,37] and alkali-heat treatment [10,11,21,38,39]. Among these processes, the alkali-heat treatment proposed by Kokubo's team [40] is a cost-effective and efficient way to induce apatite layer formation on the Ti-based alloys substrate. However, the alkali-heat treatment is a relative tedious and time-consuming process. In general, it needs a highly concentrated NaOH/KOH solution (even higher than 10 mol L^{-1}) to obtain the sodium titanate hydrogel layer (synthesis process) and a high heat-treatment temperature (up to 600°C) to crystallize the sodium titanate layer (crystallization process). On the other hand, hydrothermal treatment has been greatly developed as a simple and cost-effective technique to crystallize and form apatite coatings on the Ti alloys [41,42]. It is well-known that the hydrothermal treatment simultaneously possesses high temperature and high pressure characteristics, and can simultaneously contain synthesis and crystallization processes. Therefore, we try to use the hydrothermal treatment to replace the alkali-heat treatment to form the apatite-inducing layer on the porous Ti-Mo alloys in lower concentration NaOH solution and lower treatment temperature.

In the present study, porous Ti-15Mo alloys with different porosities were prepared by microwave sintering. The effects of ammonium hydrogen carbonate contents on the porous structure, porosity, phase composition, compressive strength, elastic modulus and bending strength of the porous Ti-15Mo alloys were investigated. Subsequently the porous Ti-15Mo alloy was treated hydrothermally in NaOH solution at 190°C for 24 h to obtain the apatite-inducing layer. At the same time, the inner and outer surface morphologies and phase composition of the hydrothermally treated sample were investigated as well as the apatite-forming ability evaluated by the immersion test in SBF solution.

MATERIALS AND METHODS

Materials preparation and characterization

Commercially available metallic Ti powders (particle size <45 μm, purity >99.9%) and Mo powders (particle size <5 μm, purity >99.95%) were used to prepare porous Ti-15 wt.% Mo alloy in this experiment. The 100 mesh sieved analytical reagent ammonium hydrogen carbonate (NH_4HCO_3) particles were mixed into the Ti-15Mo powders as the space-holder agent to adjust the porosities with the contents of 0, 5 wt.%, 15 wt.%, 25 wt.%, respectively. A schematic diagram of microwave sintering process for preparing porous Ti-15Mo alloy is shown in Fig. 1. First, the mixed Ti-Mo-NH_4HCO_3 powders were blended in a planetary ball mill (QM-3SP4, Nanjing University Instrument Plant) at speed of 200 r min^{-1} for 4 h. In order to avoid the elemental contamination from the balls and the decomposition of NH_4HCO_3 caused by temperature rise, there are no balls added into the ball-milling tank. Then, the blended powders were cold-pressed into green compact samples with two sizes of Φ20 mm×15 mm and 6 mm×6 mm×50 mm (just for bending test) through a uniaxial pressure of 260 MPa for 60 s. Subsequently, the green compact samples were put into an alumina crucible filled with β-SiC particles served as microwave susceptors to obtain more uniform temperature distribution in the compact during the microwave sintering process [27,30,43]. Then the alumina crucible was put inside a mullite fiber cotton insulation barrel. Finally, the insula-

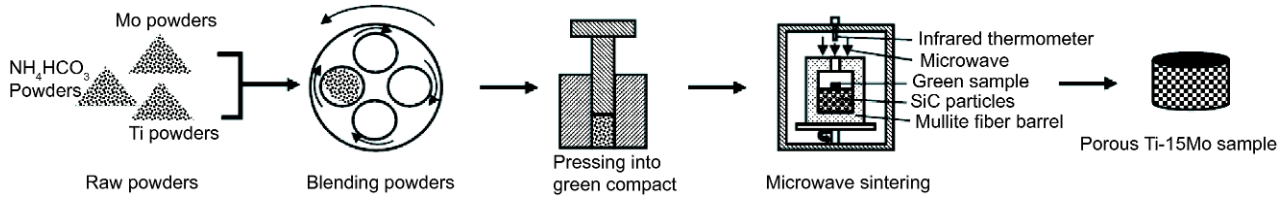

Figure 1 Schematic diagram of microwave sintering process for preparing porous Ti-15Mo alloy.

Table 1 Ionic concentrations (mmol L^{-1}) of SBF solution compared to human blood plasma

	Na^+	K^+	Mg^{2+}	Ca^{2+}	Cl^-	HPO_4^{2-}	SO_4^{2-}	HCO_3^-
SBF	142.0	5.0	1.5	2.5	148.8	1.0	0.5	4.2
Blood plasma	142.0	5.0	1.5	2.5	103.8	1.0	0.5	27.0

tion barrel was put into a 2.45 GHz, 5 kW continuously adjustable microwave equipment (NJZ4-3, Nanjing Juequan co., Ltd.) to sinter. The green compact samples were sintered by microwave heating at a rate of 20–30°C min^{-1} to 1050°C for 20 min. During the sintering process, the microwave sintering chamber was filled with high purity argon gas flow (99.999%) and a Reytek infrared pyrometer was used to measure the temperature of the sintered samples.

The phase composition of the porous Ti-15Mo alloys was identified by X-ray diffraction (XRD, Bruker D8 FOCUS, Germany). The pore structure of the porous Ti-15Mo alloys was investigated by an optical microscope (DM1500, Shenzhen HIPOWER, China) and a scanning electron microscope (SEM, FEI Quanta 200, America). The average pore sizes of the porous samples were analyzed by software of Nano Measurer 1.2 and the general porosity (P) was tested by Archimedes drainage method, calculated by the following formula:

$$P = 1 - \left(\rho / \rho_0\right), \quad (1)$$

where ρ and ρ_0 represent the density of the sintered porous Ti-15Mo alloy and the theoretical density of solid Ti-15Mo alloy, respectively; ρ/ρ_0 is the relative density. In this experiment, the theoretical density ρ_0 was 4.92 g cm^{-3}.

Mechanical properties test

Uniaxial compression tests were conducted on cylindrical porous Ti-15Mo samples with a gauge length of 10 mm and diameter of 5 mm (L/D=2.0, ASTM E9-09). The bending tests were carried out on the rectangular porous Ti-15Mo alloys with the size of 5 mm ×5 mm ×45 mm. Both of the compression tests and the bending tests were carried out at ambient temperature of 25°C with a crosshead velocity of 0.05 mm min^{-1} on Instron WDW-50 testing machine. The bending strength (σ_f) of the porous Ti-15Mo alloys could be calculated by the following formula:

$$\sigma_f = 3FL/2bh^2, \quad (2)$$

where F is the maximum loading during testing procedure, L is the span between two supports and b and h represent the breadth and height of the samples, respectively. In this test, the span L was 30 mm. For the mechanical properties test, at least five parallel tests were conducted for each group, and the results were reported as average values ± standard deviation.

Bioactive surface modification

Before hydrothermal treatment, the porous Ti-15Mo alloy prepared with 15% NH_4HCO_3 was successively polished with SiC sandpaper up to 2000 grit, and then ultrasonically cleaned in acetone and distilled water, respectively. The polished porous Ti-15Mo samples were perpendicularly mounted into the Teflon-lined stainless steel autoclaves of 50 mL capacity. The hydrothermal solution was composed of 3.75 mol L^{-1} NaOH aqueous solution and filled the Teflon container of 70% full. Finally, the autoclaves were sealed and put into drying oven to maintain 190°C for 24 h. When the hydrothermal treatment ended, the samples were taken out from the autoclaves and washed with distilled water and dried in air. To evaluate the apatite-forming ability *in vitro*, the hydrothermally treated porous Ti-15Mo alloy was immersed in simulated body fluid (SBF) solution at 37°C for 3, 7 and 14 d, respectively. The SBF solution was prepared by dissolving reagent grade NaCl, KCl, $MgCl_2{\cdot}6H_2O$, $CaCl_2$, Na_2SO_4, $NaHCO_3$, $K_2HPO_4{\cdot}3H_2O$ into distilled water. The final ionic concentrations of SBF solution (*vs.* human plasma) are listed in Table 1 [38]. The SBF solution was refreshed every 2 d to maintain the ionic concentration. The surface morphologies, elemental and

phase compositions of the hydrothermally treated and immersed porous Ti-15Mo samples were observed by SEM (FEI Nova Nano SEM450, America) equipped with energy dispersive X-ray spectrometer (EDS, INCA 250 X-Max 50, England) and XRD (Bruker D8 FOCUS, Germany), respectively.

RESULTS AND DISCUSSION

Microstructure and phase composition of porous Ti-15Mo alloys

The optical micrographs of the porous Ti-15Mo alloys with different contents of NH_4HCO_3 are shown in Fig. 2. It can be seen that a large number of pores are uniformly distributed over the surface of the samples and the pore characteristics are strongly dependent on the content of NH_4HCO_3. The pores can be divided into two categories: fine pores (<50 μm) and large pores (>100 μm). Only fine pores with the average pore size of 40 μm can be observed on the porous Ti-15Mo alloy without adding NH_4HCO_3 (Fig. 2a). On the other hand, the large quasi-circular pores are found on the surface of porous Ti-15Mo alloys after adding the NH_4HCO_3 space-holders (Fig. 2b–d), and the amount of large pores greatly increases with increasing the content of NH_4HCO_3. Moreover, the pores of the porous Ti-Mo alloys prepared with 5% NH_4HCO_3 were isolated and the connectivity among the pores is gradually enhanced with the increase of the NH_4HCO_3 contents, which results in the increase of average pore size from 120 μm for 5% NH_4HCO_3 sample to 220 μm for 25% NH_4HCO_3 sample and the formation of the three-dimensional interconnected pores. The formation of fine pores on porous Ti-15Mo alloy should be mainly attributed to the sintering necks and Kirkendall effect, which was also reported on the sintered porous NiTi alloy [44]. The diffusion rate of Mo atoms in Ti particles is much slower than that of the self-diffusivity of Ti [45], which is susceptible to the unbalanced mass transfer and the formation of Kirkendall pores [25]. The formation mechanism of the large pore is a geometrical heredity effect of space-holder NH_4HCO_3 particles [46]. During the sintering process, the NH_4HCO_3 particles will decompose into the gases of NH_3, CO_2 and H_2O, which leave the green compacts and furnace together with the continuous argon gas flow. Finally, the pores remain and the geometry of the pores nearly inherits the shape of NH_4HCO_3 particles.

In order to further analyze the microstructure of the porous Ti-15Mo alloys, the representative cross-sectional SEM images of the porous Ti-15Mo alloys prepared with

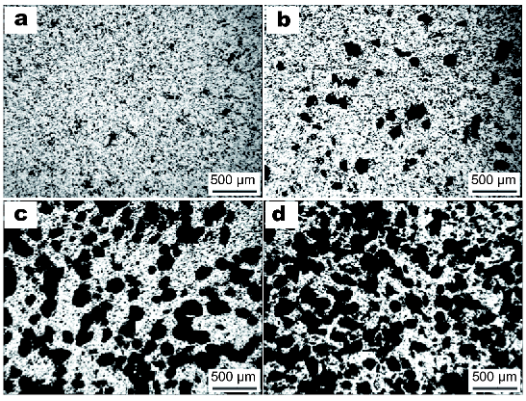

Figure 2 Optical micrographs of the porous Ti-15Mo alloys prepared by microwave sintering with different contents of NH_4HCO_3: (a) 0; (b) 5%; (c) 15%; (d) 25%.

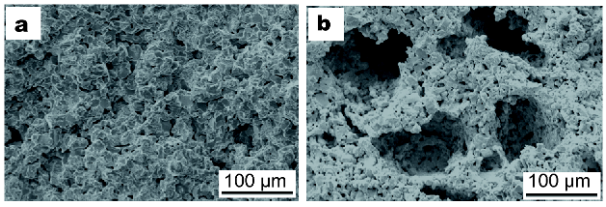

Figure 3 Cross-sectional SEM morphologies of the porous Ti-15Mo alloys prepared without NH_4HCO_3 (a) and with 15% NH_4HCO_3 (b).

and without adding NH_4HCO_3 are shown in Fig. 3. It is clear that the pore size and pore structure of porous Ti-15Mo alloy obtained from SEM are similar to the optical micrographs. However, it can be seen from Fig. 3a that the original metallic Mo powders are invisible and a large number of sintering necks are formed. The sintering necks are smooth and dense, which is beneficial to improve the mechanical properties of the sintered samples. On the other hand, a large number of fine pores are distributed over the pore wall of the large pores (Fig. 3b), which can severely degenerate the mechanical properties of the porous Ti-15Mo alloy.

Microwave sintering of metallic materials is greatly dependent on the skin depth of materials, which is the penetration depth of the microwave into the materials and can be heated directly by microwave [32]. Most metals generally possess a skin depth of the micrometer order, thus it is possible to heat them directly using powders with a particle size of the skin depth order [29,32]. Therefore, the use of near-spherical shaped Mo powders with the size of <5 μm and the use of irregular shaped Ti powders with at least one dimension of the particle matched with the skin depth of ~10 μm, could

help to absorb microwave energy quickly and thus to generate heat within the compact [29], which can greatly increase the heating efficiency and shorten the holding time. Moreover, the greatly enhanced diffusion of the atoms under the microwave field [31–33] could further accelerate the Mo diffusion into Ti and the formation of sintering necks, which might result in disappearance of original Mo powder within the shorter holding time (20 min) at lower temperature of 1050°C.

Fig. 4 shows the effect of NH_4HCO_3 contents on the porosity and density of the porous Ti-15Mo alloys. The porosities of the porous Ti-15Mo alloys linearly increase with increasing the content of NH_4HCO_3, while the densities accordingly decrease. The porosity of the porous Ti-15Mo samples without adding NH_4HCO_3 is only 16.5%, and it increases from 21.6% for 5 wt.% NH_4HCO_3 sample to 50.2% for 25 wt.% NH_4HCO_3 sample. Meanwhile, the density decreases from 4.11 g cm^{-3} (0 NH_4HCO_3 sample) to 2.45 g cm^{-3} (25% NH_4HCO_3 sample), which is very close to the density of human bone (1.8–2.1 g cm^{-3}) [47].

A large number of studies on the effects of porosity and pore size on the biological properties of the hard tissue implant materials have been reported [20,48–50]. The porosities of the Ti-15Mo alloys are in the optimal range of 20%–50% for load-bearing bone implant materials [23], which should be beneficial to the initiation of bone formation, providing enough space for bone tissue reconstruction and ingrowth [51]. Moreover, the pore sizes of the porous Ti-15Mo alloys with adding NH_4HCO_3 ranging from 120 to 220 μm are beneficial to the new bone growth, since the optimal pore size is considered to be 100–400 μm [20,52]. Therefore, the porosity and pore size of the porous Ti-15Mo alloys can be controlled within certain limits through adjusting the content of NH_4HCO_3, and the porous Ti-15Mo alloys fabricated by microwave sintering can meet the preliminary requirement for a porous implant and become a promising candidate as the bone implant.

The XRD patterns of the porous Ti-15Mo alloys with different contents of NH_4HCO_3 are graphed in Fig. 5. The porous Ti-15Mo alloys are mainly composed of body-centered cubic (bcc) β-Ti and hexagonal close-packed (hcp) α-Ti phases, revealing that the porous Ti-15Mo alloys belong to the $\alpha+\beta$ two-phase titanium alloys. According to the intensity of diffraction peaks, the porous Ti-15Mo alloys are dominated by β phase with a little α phase, and the proportion of α and β phases has no significant change as the NH_4HCO_3 content increases. No obvious diffraction peaks of elemental Mo can be detected in the porous Ti-15Mo alloys, indicating that the complete phase transformation occurred during the microwave sintering process, consistent with the results of Fig. 3. The Mo element is diffused into the Ti lattice (α-Ti), resulting in the formation of β-Ti after sintering, since Mo is a β-stabilized element. In addition, the proportion of β phase increases with increasing the Mo contents [8,25]. For the dense Ti-Mo alloys prepared by casting or smelting, the Ti-Mo alloys can obtain a fully stabilized β phase Ti alloy at room temperature after solution treatment under rapid cooling when the Mo content reaches higher than 10 wt.% [8]. However, the microwave sintered Ti-15Mo alloys are $\alpha+\beta$ two-phase titanium alloys after cooling with furnace (slow cooling), which is also consistent with the Ti-Mo binary phase diagram [10]. Similarly, the vacuum sintered porous Ti-10Mo alloy also consisted of β-Ti and α-Ti [10], and the proportion of β and α phases was much lower than that of

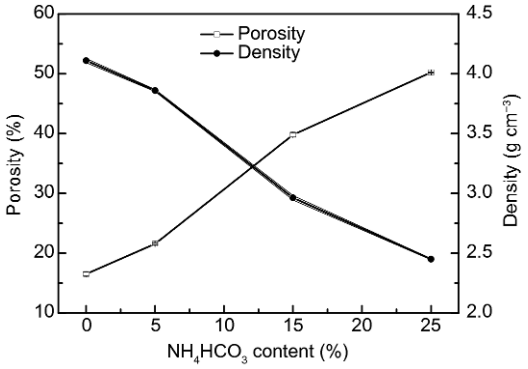

Figure 4 Effect of NH_4HCO_3 content on the porosity and density of the porous Ti-15Mo alloys.

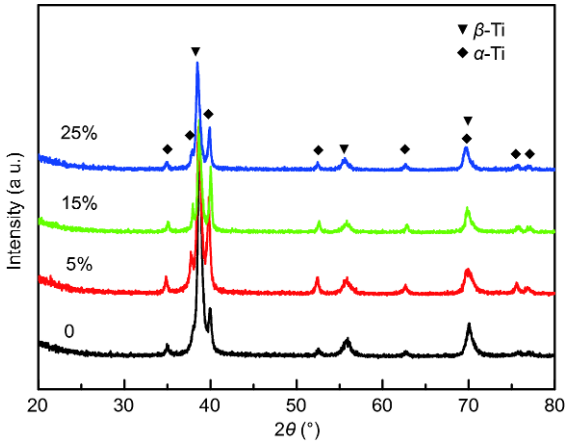

Figure 5 XRD patterns of the porous Ti-15Mo alloys with different contents of NH_4HCO_3.

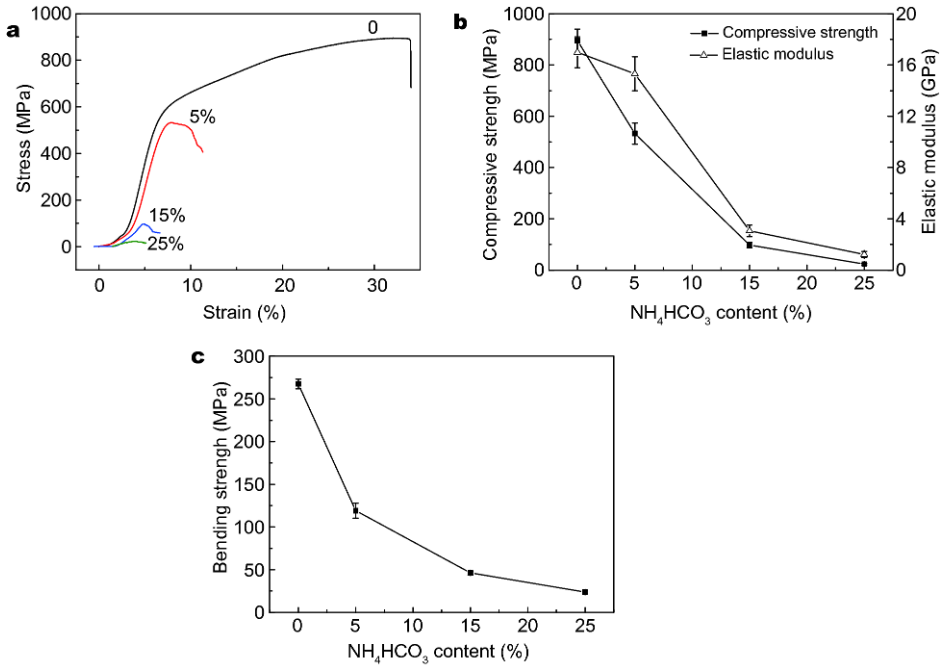

Figure 6 Compressive stress-strain curves (a), compressive strength and elastic modulus (b), and bending strength (c) of the porous Ti-15Mo alloys prepared with different contents of NH_4HCO_3.

the microwave sintered Ti-15Mo alloys according to the relative intensity of the diffraction peaks.

Mechanical properties of the porous Ti-15Mo alloys

Fig. 6a shows the nominal compressive stress-strain curves of porous Ti-15Mo alloys prepared with different contents of NH_4HCO_3. In general, the compressive process can be divided into three regions [10,28]: (i) a linear elastic deformation region, where the slope can be considered as the elastic modulus of the sample; (ii) a plastic yield deformation region, where a peak stress appears, considered as the compressive strength of the sample; (iii) a densification and rupture region, where walls of the pores will collapse and the rupture of samples occurs. As shown in Fig. 6a, when the NH_4HCO_3 content is higher than 5%, the second stage nearly disappears and no obvious deformation of stress plateau can be detected, which indicates that the compression fracture mechanism changes from ductile fracture to brittle fracture.

The compressive strength and elastic modulus of the porous Ti-15Mo alloys extracted from the stress-strain curves are shown in Fig. 6b. It can be seen that the compressive strength and elastic modulus of the porous Ti-15Mo alloys linearly decrease with increasing the NH_4HCO_3 contents. The compressive strength decreases from 895±45 MPa for 0 NH_4HCO_3 sample to 24±3 MPa for 25% NH_4HCO_3 sample. The elastic modulus also decreases from 16.09±1.21 GPa for 0 NH_4HCO_3 sample to 1.22±0.24 GPa for 25% NH_4HCO_3 sample. According to Figs 2 and 3, both the porosities and pore sizes of the porous Ti-15Mo alloys increase with increasing the NH_4HCO_3 contents. The number and thickness of pore walls decrease and the connectivity of the pore walls weakens, which leads to the decrease of the support force of the pore walls and the decrease of the compressive strength and elastic modulus. Moreover, the increase of porosities and pore sizes leads to the increase of the amount of irregular pores, which further raises the stress concentration in the porous samples and further decreases the compressive strength of the porous Ti-Mo alloy. As the load-bearing implant materials, the mechanical properties should be appropriate to match those of human bone tissue at the site of implantation [20]. In general, the compressive strength of human bone is 100–230 MPa for cortical bone and 2–12 MPa for cancellous bone [53], and the elastic modulus is 3–20 GPa for cortical bone and 0.05–0.5 GPa for cancellous bone [53]. Compared to human bone, the compressive strength and elastic modulus of the porous Ti-15Mo alloys can completely satisfy the basic mechanical requirement of the bone implant materials through adjusting the space-holder contents.

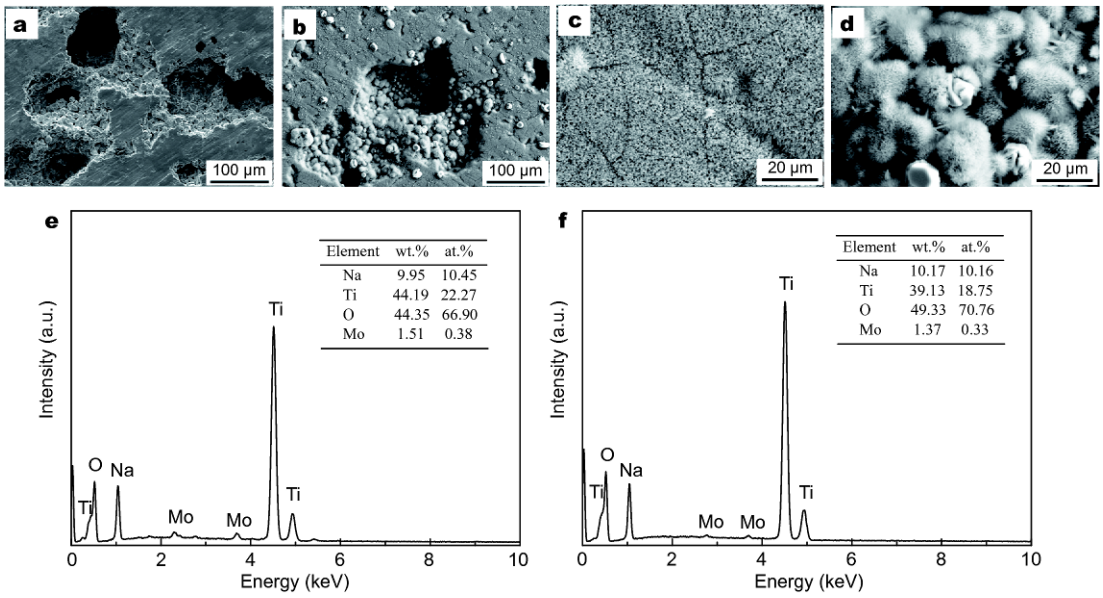

Figure 7 Surface morphologies and EDS patterns of the untreated and hydrothermally treated porous Ti-15Mo alloy samples. (a) Untreated sample; (b) hydrothermally treated sample; (c) magnification for the outer surface of the hydrothermally treated sample; (d) magnification for the inner surface of the hydrothermally treated sample; (e) EDS result of (c); (f) EDS result of (d).

The bending strength is another important mechanical property for the bone implant materials besides the compressive strength and elastic modulus. The bending strength of the porous Ti-15Mo alloys with different contents of NH_4HCO_3 is shown in Fig. 6c, and it almost linearly decreases from 267.4±5.5 MPa for 0 NH_4HCO_3 sample to 23.8±1.2 MPa for 25% NH_4HCO_3 sample with increasing the NH_4HCO_3 content, overlapping with the range of bending strength of natural cortical bone (50–150 MPa) [53]. Therefore, only considering the compressive strength, elastic modulus and bending strength, the porous Ti-15Mo alloy fabricated by microwave sintering could be a promising candidate for the hard tissue repair and replacement implant.

Due to the appropriate mechanical properties and pore structure, the porous Ti-15Mo alloy with 15% NH_4HCO_3 was chosen to carry out the surface bioactive treatment and evaluate the *in vitro* apatite-forming ability. Fig. 7 shows the surface morphologies and EDS analysis of the untreated and the hydrothermally treated porous Ti-15Mo alloy. From Fig. 7a, a large number of quasi-circular alloy particles inside and on the walls of the large pores can be observed after sintering, connected by the sintering necks, the same with Fig. 3b. After hydrothermal treatment, a film is formed on the outer surface and some fluffy sphere-like substances are generated on the inner surface, which should be transformed from the alloy particles (Fig. 7b). As shown in Fig. 7c, the film on the outer surface of the porous Ti-15Mo alloy exhibits three-dimensional needle and flake-like clusters. The inner surface of the porous Ti-15Mo alloy is also composed of needle and flake-like clusters with smaller size compared to the outer surface, as shown in Fig. 7d. According to the EDS analysis, both of the outer and inner surfaces of the porous Ti-15Mo alloy are composed of Na, Ti, O, and Mo elements (Fig. 7e, f), in which the Mo should be from the substrate. The contents of the elements on the outer surface and in the inner surface have no significant difference, indicating they form the same substances after hydrothermal treatment, only exhibiting the different needle and flake sizes. This difference should be derived from the microstructural characteristics of the porous Ti-15Mo alloy substrate, namely, smooth outer surface and alloy granular inner surface.

Fig. 8 shows the XRD pattern of the hydrothermally treated porous Ti-15Mo alloy. Besides the diffraction peaks of α-Ti and β-Ti coming from the porous Ti-15Mo alloy substrate, the diffraction peaks of a new phase $Na_2Ti_6O_{13}$ can be detected from the XRD pattern, indicating that the hydrothermally treated layer on the porous Ti-15Mo alloy is mainly composed of $Na_2Ti_6O_{13}$ crystal phase. This result is highly consistent with the EDS and the needle and flake-like clusters should be dominated by $Na_2Ti_6O_{13}$ crystal phase. Hsu *et al.* [21] reported that the

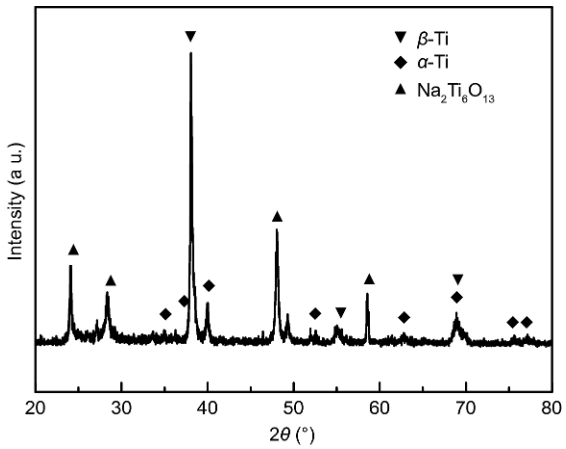

Figure 8 XRD pattern of the hydrothermally treated porous Ti-15Mo sample.

layer on the porous Ti-7.5Mo treated by alkali-heat treatment also consisted of $Na_2Ti_6O_{13}$ crystal phase. However, the diffraction peaks intensity and crystallinity of the $Na_2Ti_6O_{13}$ obtained in the hydrothermally treated sample is much higher than that of the alkali-heat treated sample. This should be attributed to the hydrothermal treatment possessing high temperature and high pressure conditions which are beneficial to the crystallization of the $Na_2Ti_6O_{13}$ phase.

During the hydrothermal treatment process, Ti reacts with the alkaline solution and forms $HTiO_3^-{\cdot}nH_2O$, followed by reacting with Na^+ in the aqueous solution to generate a sodium titanate hydrogel ($NaTiO_3{\cdot}nH_2O$) layer. The detailed chemical reaction equations are as follows [11,39]:

$$Ti + 3OH^- \rightarrow Ti(OH)_3^+ + 4e^-, \quad (3)$$

$$Ti(OH)_3^+ + e^- \rightarrow TiO_2 \cdot H_2O + 1/2H_2\uparrow, \quad (4)$$

$$Ti(OH)_3^+ + OH^- \rightarrow Ti(OH)_4, \quad (5)$$

$$Ti(OH)_4 \rightarrow TiO_2 + 2H_2O, \quad (6)$$

$$TiO_2 + OH^- \rightarrow HTiO_3^-, \quad (7)$$

$$HTiO_3^- \cdot nH_2O + Na^+ \rightarrow NaTiO_3 \cdot nH_2O + 1/2H_2\uparrow. \quad (8)$$

At last, the hydrogel layer is dehydrated under high temperature and a stable sodium titanate layer is formed in the crystal phases of $Na_2Ti_6O_{13}$ [21], Na_2TiO_{11} [38] or $Na_2Ti_3O_7$ [54], etc.

In order to evaluate the *in vitro* apatite-forming ability, the hydrothermally treated porous Ti-15Mo alloy was immersed in the SBF solution at 37°C for different times. Fig. 9 shows the surface morphologies of the hydrothermally treated porous Ti-15Mo alloy after immersed in the SBF solution for 3, 7 and 14 d, respectively, using the

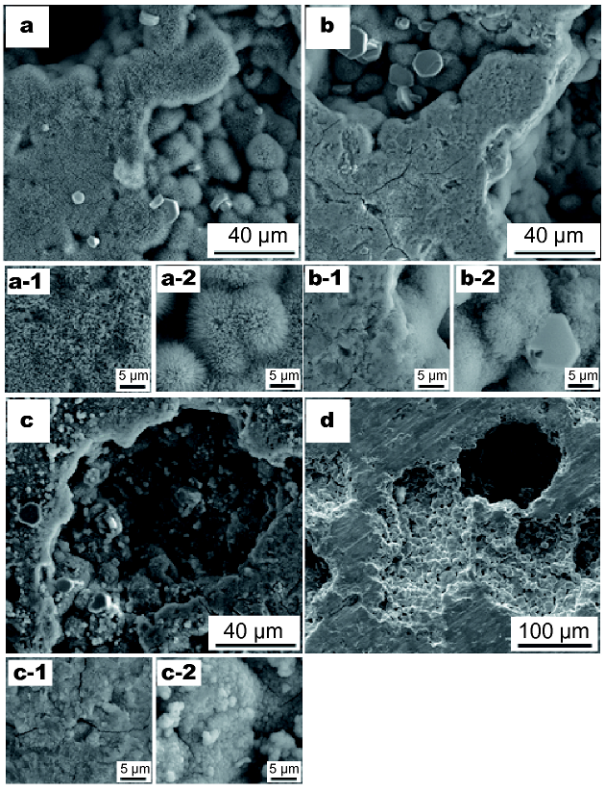

Figure 9 Surface morphologies of the hydrothermally treated porous Ti-15Mo alloy after immersed in the SBF solution for different times. (a) 3 d, (a-1) magnification for the outer surface of (a) and (a-2) magnification for the inner surface of (a); (b) 7 d, (b-1) magnification for the outer surface of (b) and (b-2) magnification for the inner surface of (b); (c) 14 d, (c-1) magnification for the outer surface of (c) and (c-2) magnification for the inner surface of (c); (d) the untreated Ti-15Mo alloy after immersed in the SBF solution for 14 d.

untreated porous Ti-15Mo alloy immersed in SBF solution for 14 d as the control. Some precipitates can be found at the tip of the clusters on the outer (Fig. 9a-1) and inner surface (Fig. 9a-2) of the porous Ti-15Mo after immersed in SBF for 3 d. With increasing the immersion time to 7 d, the precipitates greatly increase and the needle and flake-like surface morphologies of the hydrothermally treated sample nearly disappear. After further increasing the immersion time to 14 d, the entire surface of the sample is fully covered with the sphere-like precipitates, especially the inner surface (Fig. 9c-2). However, no precipitates are observed on the outer or inner surface of the untreated porous Ti-15Mo alloy after immersed in SBF solution for 14 d, as shown in Fig. 9d.

The XRD and EDS patterns of the hydrothermally treated porous Ti-15Mo sample immersed in SBF for 14 d are shown in Fig. 10. Compared with the XRD pattern of

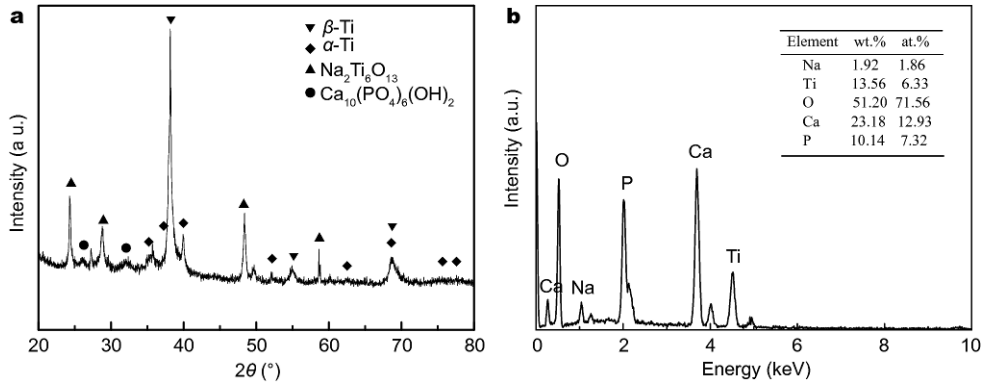

Figure 10 XRD (a) and EDS (b) patterns of the hydrothermally treated porous Ti-15Mo sample after immersed in SBF for 14 d.

the hydrothermally treated sample, two broad diffraction peaks at the 2θ=25.88° and 2θ=31°–33° can be detected from the SBF immersed sample, which are corresponding to the diffraction peaks of $Ca_{10}(PO4)_6(OH)_2$ (apatite) phase. This result indicates that the precipitates on the hydrothermally treated sample are mainly composed of apatite phase. The EDS pattern indicates that the precipitates consists of Ca, P, O, Ti, and Na elements with the atomic contents of 12.93%, 7.32%, 71.56%, 6.33% and 1.86%, respectively, in which the Ti and Na elements should be derived from the hydrothermally treated substrate. The Ca/P ratio is 1.60, slightly lower than that of stoichiometric Ca/P ratio (1.67) of apatite, which means that the induced apatite in this experiment is a Ca-deficient HA, in agreement with previous studies [30,55].

According to the results of SEM, XRD and EDS, it can be concluded that the hydrothermally treated porous Ti-15Mo alloy possesses high apatite-forming ability *in vitro*, the apatite begins to deposit after immersed in SBF for 3 d and fully covers the inner and outer surface of the porous Ti-15Mo alloy as the immersion time increased to 14 d. On the other hand, the untreated porous Ti-15Mo alloy has no apatite-forming ability and it cannot induce the apatite deposition on the sample even immersed in the SBF solution for 14 d. This result is well consistent with the previous reports [21,38], in which the porous Ti-7.5Mo alloy or as-cast Ti-7.5Mo alloy did not induce apatite deposition even after immersed in SBF for 28 d. The apatite-forming mechanism of the hydrothermally treated porous Ti-15Mo alloy is similar with the other NaOH treated Ti alloys [10,11,21,38,39]. The sodium titanate ($Na_2Ti_6O_{13}$) layers are formed on the inner and outer surface of the porous Ti-15Mo alloy after hydrothermal treatment. When the hydrothermally treated sample is immersed in the SBF solution, the Na^+ ions from the sodium titanate layers would immediately be exchanged by the H_3O^+ ions from the SBF solution, which leads to the formation of negatively charged Ti–OH groups and $HTiO_3^-$ on the surface of the sample [11,21,55]. The negative charges of Ti–OH and $HTiO_3^-$ on the sample surface can catch the Ca^{2+} through the Coulomb force and draw the HPO_4^{2-} by hydrogen bond. The Ca^{2+} and the HPO_4^{2-} can continually accumulate around the sample surface. Subsequently the concentrations of the Ca^{2+} and HPO_4^{2-} gradually increase and reach the local supersaturation, resulting in the apatite nucleation on the surface of the sample. Once the apatite nuclei are formed, they will spontaneously grow up though consuming the Ca^{2+} and HPO_4^{2-} ions from SBF solution and the apatite is largely deposited on the surface of sample finally [11,21,55]. Moreover, the inner surface of the hydrothermally treated porous Ti-15Mo alloy exhibits the better apatite-forming ability. The reason should be that the inner surface is a relative confined space and the local concentrations of the Ca and P ions inside the pores are relatively high, which is beneficial to the apatite nucleation and growth. Furthermore, the size of the needle and flake clusters on the inner surface is much smaller than that on the outer surface, thereby providing more sites to heterogeneous nucleation of the apatite.

It is well-known that the biological performance of a biomaterial obtained in the SBF method can thus be used to predict its bioactivity *in vivo* for the case of the hard tissue repair [11,30,56]. The hydrothermally treated porous Ti-15Mo alloy possesses high apatite-forming ability in SBF solution, indicating that it should possess excellent bioactivity *in vivo*. Therefore, the hydrothermal treatment is a promising candidate for the bioactive surface modification of the porous Ti-15Mo alloys.

CONCLUSIONS

Biomedical porous Ti-15Mo alloys were successfully

prepared by microwave sintering. The pore structure of the porous Ti-15Mo alloys was greatly dependent on the NH_4HCO_3 content. With increasing the contents of NH_4HCO_3, the porosities of porous Ti-15Mo alloys increased from 16.5% to 50.2% and the corresponding average pore size increased from 40 to 220 μm. The porous Ti-15Mo alloys were mainly composed of β-Ti phase with a little α-Ti phase, and the proportion of α and β phase has no significant change with increasing the NH_4HCO_3 content. The compressive strength, elastic modulus and bending strength of the porous Ti-15Mo alloys all decreased with increasing the content of NH_4HCO_3, but they could satisfy the basic mechanical requirement of the bone implant materials. After hydrothermal treatment, the needle and flake-like $Na_2Ti_6O_{13}$ layers were formed on the outer and inner surface of the porous Ti-15Mo alloy, and the hydrothermally treated porous Ti-15Mo alloy could induce the formation of the Ca-deficient apatite after immersed in SBF solution. Overall, all these results demonstrate that the hydrothermally treated porous Ti-15Mo alloy could be a promising candidate for hard tissue repair and bone implant.

Received 12 July 2017; accepted 14 August 2017; published online 27 October 2017

1 Wu S, Liu X, Yeung KWK, *et al.* Biomimetic porous scaffolds for bone tissue engineering. Mater Sci Eng-R-Rep, 2014, 80: 1–36
2 Rack HJ, Qazi JI. Titanium alloys for biomedical applications. Mater Sci Eng-C, 2006, 26: 1269–1277
3 Niinomi M. Biologically and mechanically biocompatible titanium alloys. Mater Trans, 2008, 49: 2170–2178
4 Geetha M, Singh AK, Asokamani R, *et al.* Ti based biomaterials, the ultimate choice for orthopaedic implants–A review. Prog Mater Sci, 2009, 54: 397–425
5 Krishna BV, Bose S, Bandyopadhyay A. Low stiffness porous Ti structures for load-bearing implants. Acta Biomater, 2007, 3: 997–1006
6 Nagels J, Stokdijk M, Rozing PM. Stress shielding and bone resorption in shoulder arthroplasty. J Shoulder Elbow Surgery, 2003, 12: 35–39
7 Rao S, Ushida T, Tateishi T, et al. Effect of Ti, Al, and V ions on the relative growth rate of fibroblasts (L929) and osteoblasts (MC3T3-E1) cells. Biomed Mater Eng, 1996, 6: 79–86
8 Ho WF, Ju CP, Lin JH. Structure and properties of cast binary Ti-Mo alloys. Biomaterials, 1999, 20: 2115–2122
9 Li YH, Chen RB, Qi G, *et al.* Powder sintering of porous Ti-15Mo alloy from TiH_2 and Mo powders. J Alloys Compd, 2009, 485: 215–218
10 Gao Z, Li Q, He F, *et al.* Mechanical modulation and bioactive surface modification of porous Ti-10Mo alloy for bone implants. Mater Des, 2012, 42: 13–20
11 Liu X, Chu P, Ding C. Surface modification of titanium, titanium alloys, and related materials for biomedical applications. Mater Sci Eng-R-Rep, 2004, 47: 49–121
12 Cardoso FF, Ferrandini PL, Lopes ESN, *et al.* Ti-Mo alloys employed as biomaterials: effects of composition and aging heat treatment on microstructure and mechanical behavior. J Mech Behav BioMed Mater, 2014, 32: 31–38
13 Wang BL, Li L, Zheng YF. *In vitro* cytotoxicity and hemocompatibility studies of Ti-Nb, Ti-Nb-Zr and Ti-Nb-Hf biomedical shape memory alloys. Biomed Mater, 2010, 5: 044102
14 Kuroda D, Niinomi M, Morinaga M, *et al.* Design and mechanical properties of new β type titanium alloys for implant materials. Mater Sci Eng-A, 1998, 243: 244–249
15 Zhou YL, Niinomi M. Ti-25Ta alloy with the best mechanical compatibility in Ti-Ta alloys for biomedical applications. Mater Sci Eng-C, 2009, 29: 1061–1065
16 American Society for Testing and Materials. Standard specification for wrought titanium-15 molybdenum alloy for surgical implant application, ASTM F2066-08, American Society for Testing and Materials, Philadelphia, 2008. 1–5
17 Kumar S, Narayanan TSNS. Corrosion behaviour of Ti-15Mo alloy for dental implant applications. J Dentistry, 2008, 36: 500–507
18 Somsanith N, Narayanan TSNS, Kim YK, *et al.* Surface medication of Ti-15Mo alloy by thermal oxidation: evaluation of surface characteristics and corrosion resistance in Ringer's solution. Appl Surf Sci, 2015, 356: 1117–1126
19 Yamaguchi S, Anchieta RB, Guastaldi FPS, *et al.* In silico analysis of the biomechanical stability of commercially pure Ti and Ti-15Mo plates for the treatment of mandibular angle fracture. J Oral Maxillofacial Surgery, 2017, 75: 1004.e1–1004.e9
20 Mour M, Das D, Winkler T, *et al.* Advances in porous biomaterials for dental and orthopaedic applications. Materials, 2010, 3: 2947–2974
21 Hsu HC, Wu SC, Hsu SK, *et al.* Effect of ball milling on properties of porous Ti-7.5Mo alloy for biomedical applications. J Alloys Compd, 2014, 582: 793–801
22 Lewis G. Properties of open-cell porous metals and alloys for orthopaedic applications. J Mater Sci-Mater Med, 2013, 24: 2293–2325
23 Yang D, Guo Z, Shao H, *et al.* Mechanical properties of porous Ti-Mo and Ti-Nb alloys for biomedical application by gelcasting. Procedia Eng, 2012, 36: 160–167
24 Xie F, He X, Lu X, *et al.* Preparation and properties of porous Ti-10Mo alloy by selective laser sintering. Mater Sci Eng-C, 2013, 33: 1085–1090
25 Xie F, He X, Cao S, *et al.* Influence of pore characteristics on microstructure, mechanical properties and corrosion resistance of selective laser sintered porous Ti-Mo alloys for biomedical applications. Electrochim Acta, 2013, 105: 121–129
26 Hsu HC, Wu SC, Hsu SK, *et al.* Processing and mechanical properties of porous Ti-7.5Mo alloy. Mater Des, 2013, 47: 21–26
27 Tang CY, Zhang LN, Wong CT, *et al.* Fabrication and characteristics of porous NiTi shape memory alloy synthesized by microwave sintering. Mater Sci Eng-A, 2011, 528: 6006–6011
28 Xu JL, Bao LZ, Liu AH, *et al.* Microstructure, mechanical properties and superelasticity of biomedical porous NiTi alloy prepared by microwave sintering. Mater Sci Eng-C, 2015, 46: 387–393
29 Choy MT, Tang CY, Chen L, *et al. In vitro* and *in vivo* performance of bioactive Ti6Al4V/TiC/HA implants fabricated by a rapid microwave sintering technique. Mater Sci Eng-C, 2014, 42: 746–756
30 Choy MT, Tang CY, Chen L, *et al.* Microwave assisted-*in situ* synthesis of porous titanium/calcium phosphate composites and their *in vitro* apatite-forming capability. Composites Part B-Eng, 2015, 83: 50–57

31 Mishra RR, Sharma AK. Microwave-material interaction phenomena: heating mechanisms, challenges and opportunities in material processing. Composites Part A-Appl Sci Manufacturing, 2016, 81: 78–97
32 Oghbaei M, Mirzaee O. Microwave versus conventional sintering: a review of fundamentals, advantages and applications. J Alloys Compd, 2010, 494: 175–189
33 Das S, Mukhopadhyay AK, Datta S, *et al.* Prospects of microwave processing: an overview. Bull Mater Sci, 2009, 32: 1–13
34 Kazek-Kęsik A, Krok-Borkowicz M, Pamuła E, *et al.* Electrochemical and biological characterization of coatings formed on Ti-15Mo alloy by plasma electrolytic oxidation. Mater Sci Eng-C, 2014, 43: 172–181
35 Babilas D, Służalska K, Krząkała A, *et al.* Plasma electrolytic oxidation of a Ti-15Mo alloy in silicate solutions. Mater Lett, 2013, 100: 252–256
36 Oliveira NTC, Guastaldi AC, Piazza S, *et al.* Photo-electrochemical investigation of anodic oxide films on cast Ti-Mo alloys. I. Anodic behaviour and effect of alloy composition. Electrochim Acta, 2009, 54: 1395–1402
37 Babilas D, Urbańczyk E, Sowa M, *et al.* On the electropolishing and anodic oxidation of Ti-15Mo alloy. Electrochim Acta, 2016, 205: 256–265
38 Ho WF, Lai CH, Hsu HC, *et al.* Surface modification of a low-modulus Ti-7.5Mo alloy treated with aqueous NaOH. Surf Coatings Tech, 2009, 203: 3142–3150
39 Escada ALA, Rodrigues Jr D, Machado JPB, *et al.* Surface characterization of Ti-7.5Mo alloy modified by biomimetic method. Surf Coatings Tech, 2010, 205: 383–387
40 Kim HM, Miyaji F, Kokubo T, *et al.* Preparation of bioactive Ti and its alloys *via* simple chemical surface treatment. J Biomed Mater Res, 1996, 32: 409–417
41 Ou SF, Wang CY. Fabrication of a hydroxyapatite-containing coating on Ti-Ta alloy by electrical discharge coating and hydrothermal treatment. Surf Coatings Tech, 2016, 302: 238–243
42 Liu F, Song Y, Wang F, *et al.* Formation characterization of hydroxyapatite on titanium by microarc oxidation and hydrothermal treatment. J Biosci Bioeng, 2005, 100: 100–104
43 Liu X, Zhang Z, Wu Y. Absorption properties of carbon black/silicon carbide microwave absorbers. Composites Part B-Eng, 2011, 42: 326–329
44 Li BY, Rong LJ, Li YY. The influence of addition of TiH_2 in elemental powder sintering porous Ni-Ti alloys. Mater Sci Eng-A, 2000, 281: 169–175
45 Liu Y, Chen LF, Tang HP, *et al.* Design of powder metallurgy titanium alloys and composites. Mater Sci Eng-A, 2006, 418: 25–35
46 Li DS, Zhang YP, Ma X, *et al.* Space-holder engineered porous NiTi shape memory alloys with improved pore characteristics and mechanical properties. J Alloys Compd, 2009, 474: L1–L5
47 Staiger MP, Pietak AM, Huadmai J, *et al.* Magnesium and its alloys as orthopedic biomaterials: a review. Biomaterials, 2006, 27: 1728–1734
48 Itälä AI, Ylänen HO, Ekholm C, *et al.* Pore diameter of more than 100 μm is not requisite for bone ingrowth in rabbits. J Biomed Mater Res, 2001, 58: 679–683
49 Bertheville B. Porous single-phase NiTi processed under Ca reducing vapor for use as a bone graft substitute. Biomaterials, 2006, 27: 1246–1250
50 Kujala S, Ryhänen J, Danilov A, *et al.* Effect of porosity on the osteointegration and bone ingrowth of a weight-bearing nickel-titanium bone graft substitute. Biomaterials, 2003, 24: 4691–4697
51 Li JP, Li SH, Van Blitterswijk CA, *et al.* A novel porous Ti6Al4V: characterization and cell attachment. J Biomed Mater Res, 2005, 73A: 223–233
52 Barrabés M, Sevilla P, Planell JA, *et al.* Mechanical properties of nickel-titanium foams for reconstructive orthopaedics. Mater Sci Eng-C, 2008, 28: 23–27
53 Hench LL. Bioceramics. J Am Ceramic Soc, 2005, 81: 1705–1728
54 Sasikumar Y, Rajendran N. Influence of surface modification on the apatite formation and corrosion behavior of Ti and Ti-15Mo alloy for biomedical applications. Mater Chem Phys, 2013, 138: 114–123
55 Kokubo T, Kim HM, Kawashita M. Novel bioactive materials with different mechanical properties. Biomaterials, 2003, 24: 2161–2175
56 Kokubo T, Takadama H. How useful is SBF in predicting *in vivo* bone bioactivity? Biomaterials, 2006, 27: 2907–2915

Acknowledgements This work was supported by the National Natural Science Foundation of China (51101085), the Aeronautical Science Foundation of China (2015ZF56027), the Natural Science Foundation of Jiangxi Province (2016BAB206109), the Science and Technology Support Plan Project of Jiangxi Province (20151BBG70039), and the Science and Technology Project of Jiangxi Province Education Department (GJJ150721).

Author contributions Xu J designed the experiments; Zhang J and Bao L performed the experiments; Bao L and Lai T performed the data analysis; Xu J wrote the paper with support from Bao L; Luo J and Zheng Y contributed to the theoretical analysis. All authors contributed to the general discussion.

Conflict of interest The authors declare that they have no conflict of interest.

Jilin Xu is currently an associate professor at the School of Materials Science and Engineering, Nanchang Hangkong University. He was born in Ningdu, Jiangxi province, China, in 1982. He received his PhD degree in materials physics and chemistry from Harbin Institute of Technology, China, in 2009. His research focuses on the biomedical metallic materials and the corrosion and protection of metals.

Yufeng Zheng received his PhD in materials science from Harbin Institute of Technology, China, in 1998. Since 2004, he has been a full professor at Peking University in Beijing, China. His research focuses on the development of various new biomedical metallic materials (biodegradable Mg, Fe and Zn based alloys, β-Ti alloys with low elastic modulus, bulk metallic glass, ultra-fine grained metallic materials, etc.).

生物医用多孔Ti-15Mo合金的微波烧结制备及表面活性处理

徐吉林[1*], 张金龙[1], 鲍路姿[1], 赖涛[1], 罗军明[1], 郑玉峰[2*]

摘要 本文采用微波烧结制备了生物医用多孔Ti-15Mo合金，并以碳酸氢铵为造孔剂调节合金孔隙率及力学性能. 多孔Ti-15Mo合金是由主晶相β-Ti和少量α-Ti组成，其中α/β的比例随碳酸氢铵含量的增加无明显变化. 随着碳酸氢铵含量的增加，多孔Ti-15Mo合金的孔隙率和孔径均随之增加，而抗压强度、弹性模量和抗弯强度随之下降. 然而，合金的抗压强度、抗弯强度和弹性模量均高于或接近于自然骨. 采用水热法对多孔Ti-15Mo合金进行表面活化处理后，多孔Ti-15Mo合金外表面和内表面均形成了针片状的$Na_2Ti_6O_{13}$涂层. 水热处理试样经SBF溶液浸泡14天后，内外表面均完全被缺钙的磷灰石层所覆盖，说明水热处理的多孔Ti-15Mo合金具有优异的磷灰石形成能力和生物活性. 由此可见，水热处理的微波烧结多孔Ti-15Mo合金是一种非常有前途的骨植入材料.

